Available online at www.sciencedirect.com
SCIENCE DIRECT
Polymer 46 (2005) 11716–11727
polymer
www.elsevier.com/locate/polymer

Influence of montmorillonite layered silicate on plasticized poly(L-lactide) blown films

Christopher Thellen [a], Caitlin Orroth [a], Danielle Froio [a], David Ziegler [a], Jeanne Lucciarini [a], Richard Farrell [b], Nandika Ann D'Souza [c], Jo Ann Ratto [a,*]

[a] US Army Natick Soldier Center, Nanomaterials Science Team and Advanced Processing Team, Kansas Street, Natick, MA 01760-5020, USA
[b] Department of Soil Science, University of Saskatchewan, Saskatoon, Saskatchewan, SK, Canada S7N5A8
[c] Department of Materials Science and Engineering, University of North Texas, Denton, TX 76203, USA

Received 1 April 2005; received in revised form 7 September 2005; accepted 9 September 2005
Available online 14 October 2005

Abstract

Plasticized poly(L-lactide) (PLA) montmorillonite layered silicate (MLS) nanocomposites were compounded and blown-film processed using a co-rotating twin screw extruder. PLA was mixed with 10 wt% acetyltriethyl citrate ester plasticizer and 5 wt% of an organically modified montmorillonite at various screw speeds. Wide-angle X-ray diffraction (WAXD) and transmission electron microscopy (TEM) determined that the compounded pellets and the blown film PLA/MLS nanocomposites were intercalated. The effect of processing screw speeds on the barrier, thermal, mechanical, and biodegradation properties of the nanocomposites were analyzed and compared to the neat polymer. Nanocomposite films show a 48% improvement in oxygen barrier and a 50% improvement in water vapor barrier in comparison to the neat PLA. The thermogravimetric analysis (TGA) showed an overall 9 °C increase in the decomposition temperature for all of the nanocomposites. Differential scanning calorimetry (DSC) has determined that the glass transition, cold crystallization and melting point temperatures were not significantly influenced by the presence of MLS. Mechanical properties of the nanocomposites showed that the Young's modulus increased by 20% and the ultimate elongation of the nanocomposites were not sacrificed in comparison to the neat samples. Biodegradation rates in soil were slightly greater for the PLA/MLS nanocomposite than the pure PLA. However, none of the PLA pure and nanocomposites achieved significant biodegradation levels after 180 days.

Keywords: Polylactide; Montmorillonite; Nanocomposites; Biodegradation; Barrier properties

1. Introduction

Nanocomposites consisting of polymers with montmorillonite layered silicates (MLS) has become a highly publicized area of research [1–8]. It has been shown that high aspect ratio particles such as MLS, which have at least one dimension in the nanometer range, may improve the properties of the polymer significantly. The MLS commonly used in these nanocomposites is organically modified montmorillonite, a mica-type silicate, which consists of sheets arranged in a layered structure. MLS are used due to their high cation exchange capacity and high surface area (approximately 750 m^2/g and large aspect ratio (greater than 50) with a platelet thickness of 10 Å). The large aspect ratio of the silicate layers results in a high interfacial area. This increase in the interface minimizes the chain mobility, creating a reinforcement effect. In addition, this interface facilitates stress transfer to the reinforcement phase, thus improving physical properties such as tensile strength and tensile modulus [1,5]. The degree of property enhancement depends on the degree of intercalation/exfoliation of the nanocomposite. The organically modified MLS must interact with the polymer and be dispersed throughout the organic matrix for the physical properties to improve. The highest degree of property enhancement is seen in exfoliated structures where individual platelets move apart from other layers. Intercalation occurs when the polymer chains find their way between MLS platelet layers. In comparison to other more conventional composites with high loading levels (>30 wt%), nanocomposites use significantly smaller loadings (1–5 wt%) to achieve similar, if not better, results [1,4]. More importantly for food packaging applications, these high aspect ratio nanolayers can potentially force gas and water molecules to follow a more tortuous path through the polymer matrix.

* Corresponding author. Tel.: +1 508 233 5315; fax: +1 508 233 5521.
E-mail address: joann.ratto@natick.army.mil (J.A. Ratto).

0032-3861/$ - see front matter © 2005 Elsevier Ltd. All rights reserved.
doi:10.1016/j.polymer.2005.09.057

This results in much larger diffusion distances, thereby lowering permeability [1,4].

For our purposes, the potential application is environmentally friendly food packaging films for the military. Thus, the polymer of choice was poly(L-lactic) acid (PLA), which is typically formed through the fermentation of corn and corn-based products. The hydrolysis of this polymer back into its monomer state provides a major advantage over many petroleum-based polymer resins. PLA's biodegradable nature makes this polymer popular for biomedical applications such as sutures, bone screws, and scaffolding for tissue engineering [9]. Other advantages of PLA include high gloss and clarity, high tensile strength, low coefficient of friction, and high deadfold and twist retention; which make it a good choice for packaging, candy wrappers, beverage cups, bread bags, and short shelf-life bottle applications [9]. However, its high glass transition temperature (55 °C) makes it relatively stiff at room temperature. Thus, a plasticizer is frequently required to promote flexibility and processing control [10–12]. Combining PLA with MLS may result in a nanocomposite with barrier properties that are suitable for a film packaging material.

Whereas several PLA nanocomposite studies can be found in the literature, none of these has focused on citrate–ester plasticized blown film nanocomposites. Polylactide-based nanocomposites were first prepared through solvent-casting by Ogata [13]. However, transmission electron microscopy (TEM) and wide-angle X-ray diffraction (WAXD) techniques revealed that only microcomposites were formed and that an intercalated morphology was not achieved. The paper also states that the MLS in the nanocomposite acted as a nucleating agent for crystalline growth. Young's modulus did not increase significantly because the silicate layers were not dispersed [13]. Ray and co-workers [14–20] recently published a series of articles on PLA/silicate nanocomposites processed through twin-screw melt extrusion and compression molding. They reported successful enhancements in practical material properties such as storage modulus, flexural strength, heat distortion temperature, and overall biodegradability of the nanocomposites. Paul and co-workers [21,22] also reported successful preparation of PLA/montmorillonite nanocomposites through melt blending and compression molding. They used 3% organically modified and unmodified montmorillonite layered silicates (Closite 25A, 20A and 30B) and polyethylene glycol as a plasticizer to enhance film flexibility. In both studies, the resulting nanocomposites displayed intercalated nanostructures. Vasanthan [23] worked with PLA and montmorillonite by preparing a PLA/MLS solution, casting films, and melt pressing them. The MLS served as a nucleating agent, showing a 50 °C increase in T_m using both L- and D-lactic acid stereoisomers of PLA. Chang et al. [24] reported incorporating 2–8% modified montmorillonite into PLA by solution intercalation methods—comparing two different montmorillonites with respect to thermal and mechanical properties. The tensile modulus increased with montmorillonite content while the tensile strength decreased after the addition of 4% (w:w) montmorillonite. Maiti et al. [25] also investigated PLA melt extruded nanocomposites with montmorillonite, observing an increase in storage modulus of up to 40% at clay loadings of only 2–3% compared with the pure PLA. Cook [26] designed surface-functional nanoparticles and dispersed them in PLA to improve barrier properties and hardness without loss of toughness or flexibility. Krikorian [27] has studied the crystallization behavior of PLA/MLS cast films with two different MLS's (Closite 15A and 30B). He used high concentrations of MLS (10–15% by weight) and studied spherulite growth rates and crystallization kinetics in exfoliated versus intercalated systems.

Whereas each of these studies has contributed significantly to our understanding of PLA nanocomposites, improvements in mechanical, thermal and barrier properties have been relatively limited. Since the processing parameters of screw configuration, screw speed, temperature and residence time during melt processing of nanocomposites has been found to alter the interaction of the polymer and nanoparticle [8], in this present study, melt processing is explored for a PLA/MLS system. Our prior work on ethylene *co*-vinyl alcohol nanocomposites indicated that blown film processing renders improved properties compared to nanocomposite films formed from cast extrusion [28]. The bi-axial orientation of blown-film processing presumably improves dispersion of the MLS platelets and orients them in the polymer matrix. Biaxial orientation of the polymer matrix itself can affect mechanical properties, such as modulus and stiffness, increasing in the direction of orientation [29]. Increased molecular orientation also reduces permeability, thus yielding enhanced barrier properties [30]. Indeed, in previous studies of cast vs. blown films of nanocomposites we have shown that orientation of the MLS platelets is better for blown films, yielding better barrier and mechanical properties [28].

The objective of this study was to conduct a detailed analysis of plasticized PLA/MLS nanocomposites produced through the blown-film process. To the best of our knowledge, there has been no reported research in blown-film processing of plasticized PLA/MLS nanocomposites. Based on research by Martin and LaBrecque, who studied biodegradation of PLA with different plasticizers, a 10% loading of acetyl triethyl citrate was chosen as the concentration and plasticizer for this PLA nanocomposite blown film study [11,12]. Extensive work reported previously was carried out to determine a compatible organically modified MLS, an optimum MLS concentration for the PLA and the influence of varying the screw configurations [31,32]. Incorporation of nanosized MLS platelets into the PLA polymer matrix should improve the barrier, mechanical, and thermal properties of the resulting film to the extent that they meet the diverse needs of the packaging industry, while providing an environmentally-friendly material that is commercially producible through blown-film processing methods.

2. Experimental

2.1. Materials

Poly(L-lactide) polymer 4041D, a product of Natureworks™, was supplied by Cargill/Dow LLC (Minnetonka,

MN) for use as the polymer matrix in the nanocomposite. This blown-film grade of PLA has a reported molecular weight of 180,000 Daltons along with 95% L-content and 5% D-content. Acetyltriethyl citrate, Citroflex A-2 (MW = 318 Daltons) was purchased from Morflex (Greensboro, NC) as a liquid plasticizer for PLA.

An organically modified MLS was provided by Southern Clay Products (Gonzales, TX). The MLS employed in this work is Cloisite 25A, which is a natural montmorillonite modified with a quarternary ammonium salt. The organic modifier is dimethyl, hydrogenated tallow, 2-ethylhexyl quaternary ammonium. This modified MLS was chosen based on a mini-extruder processing study where several gram size formulations of the PLA and various modified MLS's were processed with a twin screw mini-extruder and characterized using X-ray diffraction and Transmission electron microscopy (TEM) for interactions, dispersion and compatibility [31].

2.2. Nanocomposite pelletization

PLA and MLS were compounded into pellets on a Thermoprism TSE-16 co-rotating, twin-screw extruder with an attached strand die, cooling bath, and pelletizer. This machine is a co-rotating; completely intermeshing, twin-screw extruder with a 16 mm bore size and a *L*/*D* ratio of 24:1. The dried PLA pellets were fed into the extruder by the primary feeder located in the feed zone of the extruder. The MLS was then added to the extruder through the second vent port by way of a Brabender DSR 28N secondary volumetric feeder located downstream of the extruder. The twin-screw configuration was set to yield a normal shear process. Nanocomposite strands were pulled through a water bath at 20 °C and cut into pellets using a Thermoprism LPT-16 pelletizer and air knife. The pure PLA was processed in the same fashion so that the control would have the same thermal history as the nanocomposite pellets. The barrel temperature of the extruder ranged from 210 °C in the feed zone to 225 °C in the metering zone.

2.3. Blown film processing

To prepare for blown film processing, the compounded PLA/MLS resin and the control PLA resin were dried for 4 h at 80 °C to remove moisture absorbed during the pelletizing process. The resin was allowed to cool to room temperature for 1 h, after which 10 wt% plasticizer was added to the pellets and mechanically mixed for 20 min. The pellets and plasticizer were then allowed to sit for 2 h so that the pellets could absorb the plasticizer.

The plasticized polymer pellets were loaded into the extruder hopper of the 16-mm co-rotating twin-screw extruder (ThermoPrism) and fed by way of the primary volumetric feeder. A spiral flow blown-film die with a 25.4 mm diameter was used to produce the film. The blow-up ratio (BUR) of the bubble was 2:1. This setting produced a bubble with an average film thickness of 0.076 mm (~0.003 in.). Films were cooled using a single lip air ring.

Table 1
Processing conditions for blown film

Sample name	Screw speed (rpm)	Feed rate (g/min)	Die temp. (°C)
Neat no. 1	80	40.5	175
Neat no. 2	110	40.5	175
Neat no. 3	130	40.5	175
Neat no. 4	80	48.5	175
Nano no. 1	80	40.5	165
Nano no. 2	110	40.5	165
Nano no. 3	95	40.5	165
Nano no. 4	80	48.5	165

To examine how processing parameters affected both the PLA/MLS interactions and the film properties, the screw speed and feeding rate were varied during the blown film process. The temperature of zones 1, 2, 3 and 4 were 150, 155, 160 and 165 °C, respectively, while the die temperature was varied from 165 to 175 °C. The screw speed was set at 80, 110 or 130 rpm to produce neat PLA blown-films as well as nanocomposite blown-films. Note that all films contained the plasticizer since pure PLA films are difficult to process without a plasticizer. Table 1 lists the specific films that were produced and the processing conditions used to produce them. All films labeled as 'Neat' contain only the PLA polymer and plasticizer (10 wt%). Films labeled 'Nano' contain PLA polymer, plasticizer (10 wt%) and MLS 25A (5 wt%).

2.4. Methods of analysis

2.4.1. Wide angle X-ray diffraction

Wide angle X-ray diffraction (WAXD) was performed to determine the degree of intercalation and/or exfoliation of each PLA/MLS nanocomposite, using a Scintag XDS 2000 Diffractometer. The conditions of XRD analysis were: 42 mA, 47 kV; Tube fixed slits: scatter 4 mm, divergence 2 mm; detector fixed slits: scatter 0.5 m; scan range: 1.00–11.98° 2(; scan rate: 1.00°/min; step size: 0.030°/min; time step: 1.800 s; scan mode: continuous.

2.4.2. Transmission electron microscopy

For transmission electron microscopy (TEM), samples of PLA pellets and blown film were first prepared by cutting thin (~200 nm) slices of the samples. The PLA pellets were precut into a pyramid shaped point and then ultra-microtomed at room temperature, with the sections placed onto porous carbon film coated TEM grids. The blown film PLA sample was embedded in TEM grade epoxy, then precut and ultra-microtomed at room temperature. Once on the TEM grids, the PLA samples were loaded into a liquid-nitrogen cooled cryogenic TEM holder and imaged in the TEM with the samples maintained at a temperature of −60 °C to prevent the samples from burning in the TEM.

The ultra-microtome used was a Leica model Ultracut UCT with cryo-attachment EM-FCS with diamond knives used for both room temperature and cryogenic cutting. The TEM is a JEOL FasTEM 2010, operated at 200 keV with a LaB_6

filament; the digital images were recorded on a 1×1 K digital camera attached to the GIF (Gatan Image Filter). The cryoholder was a Gatan model 613 cold stage with the SmartSet temperature controller.

The TEM images were analyzed using Image J (registered trademark sign). The pixel count corresponding to the scale was noted. Line profiles across the dark lines of the MLS platelets were measured and the line thickness calculated from the pixel-scale correlation. The thickness of the lines was measured for 15 dark lines and the average noted. Line thicknesses were divided by the *d*-spacing to determine the number of platelets in each line.

2.4.3. Barrier testing

Water vapor barrier testing and oxygen barrier testing were carried out in accordance with ASTM Standards F1249-99 and D3985-99, respectively. Water vapor transmission was measured using a Modern Controls Inc. (MOCON) Perma-Tran 3/33 and a humidified nitrogen flow rate of 100 cm^3/min at 90% relative humidity and 37.8 °C. Oxygen transmission was measured using a MOCON Ox-Tran 2/20 with an oxygen flow rate of 20 cm^3/min at 0% relative humidity and 23 °C. Water vapor and oxygen permeation rate testing were carried out at atmospheric conditions.

2.4.4. Thermogravimetric analysis

Thermogravimetric analysis (TGA) was performed using a TA Instruments Hi-Res 2950 TGA apparatus. The percent weight loss was recorded as a function of temperature at a heating rate of 20 °C/min from room temperature to 800 °C in a nitrogen-filled environment.

2.4.5. Differential scanning calorimeter

The DSC measurements were conducted on a Perkin Elmer DSC-6 working on a Pyris platform. Each sample (5–10 mg) was run at a scanning rate of 10 °C/min in a nitrogen atmosphere. Samples of indium and cyclohexane were used to calibrate the DSC. Samples were heated from 30 to 180 °C at 10 °C/min, annealed for 20 min at 180 °C and cooled to 30 °C at a rate of 10 °C/min. The scan cycle was then repeated.

2.4.6. Optical microscopy

To understand the MLS macro-dispersion in the film, optical microscopy (OM) was conducted using a Zeiss optical microscope at 40× magnification. All pictures were taken using a CONTAX camera. The images were also analyzed using polarized light to determine PLA spherulitic structure. The film was heated to 180 °C and cooled to 115 °C, at which temperature it was annealed, and then cooled to room temperature and images were collected.

2.4.7. Mechanical testing

Tensile testing of the blown film samples was carried out according to ASTM Standard D882-99 on an Instron 1130 equipped with a 200 lb load cell. The gauge length of the test samples was 50.8 mm, and the width of the samples was 13.8 mm. The crosshead speed of the test was maintained at 50.8 mm/min during the duration of each test. Due to the width of the film samples formed through blown-film processing (1.8–2 in.), only the tensile properties in the machine direction of the film could be tested accurately for this experiment.

2.4.8. Biodegradation testing using a soil respirometry test

The ultimate biodegradability (i.e. mineralization) of the PLA/MLS nanocomposites was assessed using standard laboratory scale reactors to simulate a bioactive soil burial site. All film samples were cryogenically milled into powder for the testing. Prior to testing, appropriate sub-samples of each material were dried to a constant weight in a convection oven (50 °C for 12–18 h) and cooled to room temperature in a desiccator.

Polymer mineralization studies were conducted using a static soil biometer system incorporating elements of both the soil biometer system of Bartha & Pramer and ASTM standard D 5988 [33,34]. The soil used was a standard soil mix composed of a 1:1:0.1 (w:w:w) mix of potting soil, sand, and composted manure (water holding capacity = 46.4 g H_2O per 100 g soil; pH 7.0; C:N ratio = 17:1). Test samples yielding a substrate loading of 5.0 mg C g^{-1} soil were mixed with the soil; buried in test reactors (1-L mason jars fitted with Plexiglas compression lids and a Swagelok gas sampling port) containing 75 g of soil at a water content of 60% water-holding capacity (Whc); and incubated in a controlled environment chamber at 22 ± 1 °C in the dark. Soil water content was maintained at 55 ± 5% Whc by periodically watering the soils with either sterile tap water or dilute (1/2-strength) Hoagland's solution.

Samples of the headspace gas were withdrawn from the reactors at 12–120 h intervals and analyzed for CO_2 content using a Varian Model CP2003 Micro-GC equipped with a Poraplot U column and a micro-TCD (thermal conductivity detector). Each time the headspace gas was sampled, the systems were aerated by allowing the atmosphere in the bioreactors to exchange and equilibrate with atmospheric air for 5–10 min; at the same time, the soils were hand-mixed to ensure that anaerobic microenvironments did not develop. Daily and cumulative CO_2 production (total and net) were then calculated relative to a control reactor (soil without added polymer). In addition, net mineralization of a positive control (i.e. microcrystalline cellulose; Sigma Chemical Corp., St Louis, MO) was monitored to ensure that the soil supported an actively degrading microbial population throughout the test exposure. All analyses were run in triplicate.

Biodegradation data were plotted in the form of net CO_2 production vs. time curves and analyzed using a combination of linear (firstst order polynomial) and non-linear (three-parameter, single exponential rise to a maximum) regression techniques. Test results were interpreted in terms of the response parameters described by Farrell et al. [35].

3. Results and discussion

3.1. Effect of processing on montmorillonite dispersion

The degree of polymer/MLS intercalation was assessed using both X-ray and TEM methodologies to provide a more precise idea of the morphology. Fig. 1 illustrates the difference in WAXD patterns related to processing. It is clear that a shift to lower 2θ values is observed in all nanocomposite samples. The corresponding *d*-spacings are tabulated in Table 2. Both the pellets and processed films indicated an intercalated dispersion with the *d*-spacing corresponding to the (001) reflection of the MLS doubling from 18.7 to 35 Å for the pellets. The degree of intercalation in the films was slightly lower with a *d*-spacing of 32 Å. There was no significant process induced effects to be discerned in the XRD. The TEM images corresponding to the samples corroborate the XRD measurements.

As seen in Fig. 2 for the pellets and Fig. 3 for a blown film sample, the dispersion is significant. First we consider the low magnification images (2a and 3a). Indeed, at low magnification the MLS platelets are seen to be randomly dispersed, with some orientation of the platelets in the blown film nanocomposite (Fig. 3a). Clearly, the nanocomposite films exhibit the same morphological features as the pellets, including tactoid formation, intercalation (Fig. 4b), and dispersion of the platelets throughout the polymer matrix. Line thicknesses were calculated using Image J and correspond to 170–200 Å at lower magnification. Thus it can be seen that each line corresponds to a stack of around 6 platelets. This inference is supported by the higher magnification images (2b and 3b) which show well separated lines of a few platelets corresponding to a single dark line at low magnifications. The MLS platelets appear to be oriented in one direction which is induced in the film during processing; however, there also appear to be MLS tactoids that are near the separated MLS platelets (Figs. 2c and 3c).

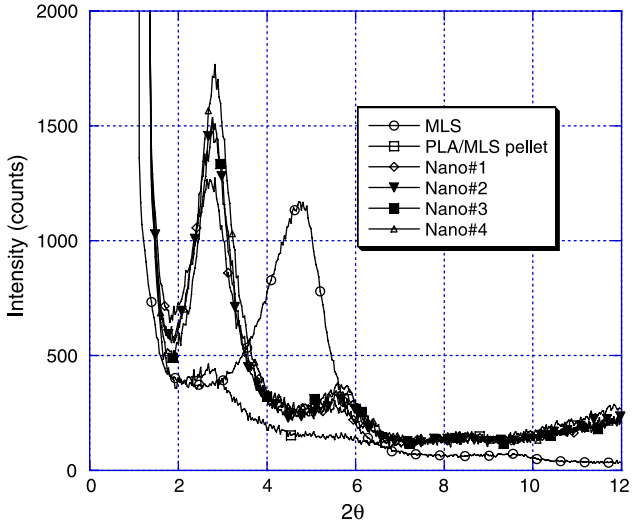

Fig. 1. WAXD patterns for the blown film nanocomposites.

Table 2
MLS platelet *d*-spacing of PLA/MLS nanocomposites

Material	*d* (Å)
MLS	18.7
PLA/MLS-pellet	35.0
Nano no. 1	32.0
Nano no. 2	32.2
Nano no. 3	31.7
Nanono. 4	31.5

3.2. Barrier performance to oxygen and water vapor

The potential for enhanced barrier performance of the nanocomposite films relative to the neat films is a reflection of the large aspect ratio and surface area of the MLS. That is, when dispersed sufficiently, these platelets may form a 'tortuous pathway' that oxygen and water molecules must follow to permeate through the film. The tortuous path theory is based on the premise that a molecule must follow a more complicated path when MLS is dispersed throughout the polymer matrix than when the matrix consists of the homopolymer alone. Research has shown, however, that the degree of tortuosity also reflects geometrical influences such as the shape and state of exfoliation/intercalation of the platelets and their orientation in the polymer matrix [36,37]. For example, working with compression molded PLA and PLA-nanocomposites, Ray and co-workers [16] reported no significant decrease in oxygen permeability of the nanocomposite and suggested that the planar orientation of the dispersed nanoparticles in the compression-molded films did not adequately increase the tortuosity of the matrix. We hypothesized that the biaxial orientation of MLS platelets in the PLA matrix produced during the blown film process would increase tortuosity enough to produce enhanced barrier properties.

Permeation results from MOCON testing of the neat and nanocomposite films are presented in Fig. 4. In all cases, the nanocomposite films were better oxygen barriers than the pure PLA films (Fig. 4a), exhibiting a 15–48% reduction in oxygen permeation rate. However, the oxygen permeation rate of the nanocomposite films was essentially independent of screw speed and feed rate, suggesting that this rate is controlled by the MLS component of the films. Conversely, the oxygen barrier properties of the PLA homopolymer were quite sensitive to processing. For instance, a modest increase in screw speed from 80 rpm (Neat no. 1) to 110 rpm (Neat no. 2) produced a 35% decrease in the oxygen permeation rate. Further increasing the screw speed to 130 rpm (Neat no. 3), however, resulted in films with increased oxygen permeation rate. Changing the feed rate had a similar effect on the oxygen barrier properties of the pure PLA films. These results suggest that the need to optimize processing parameters is more critical when working with the PLA homopolymer than when working with the PLA/MLS nanocomposite.

The PLA/MLS nanocomposites also exhibited much improved barrier properties to water vapor relative to the neat films (Fig. 4b). In general, incorporating MLS 25A into

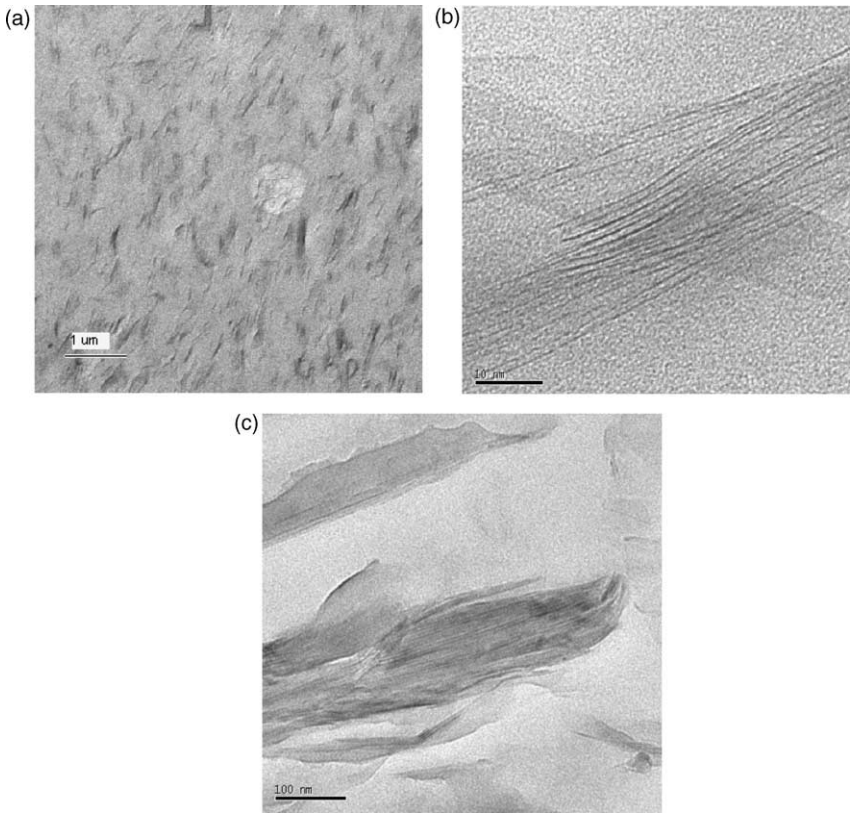

Fig. 2. TEM of the PLA-25A compounded pellet: (a) low magnification, (b) high magnification, (c) medium magnification.

the PLA matrix decreased the permeation rate of the resulting films to water vapor by about 40–50% [33]. Presumably, as water penetrates the MLS surface, forming water clusters in the nanocomposites [38,39], the diffusivity and overall transport of

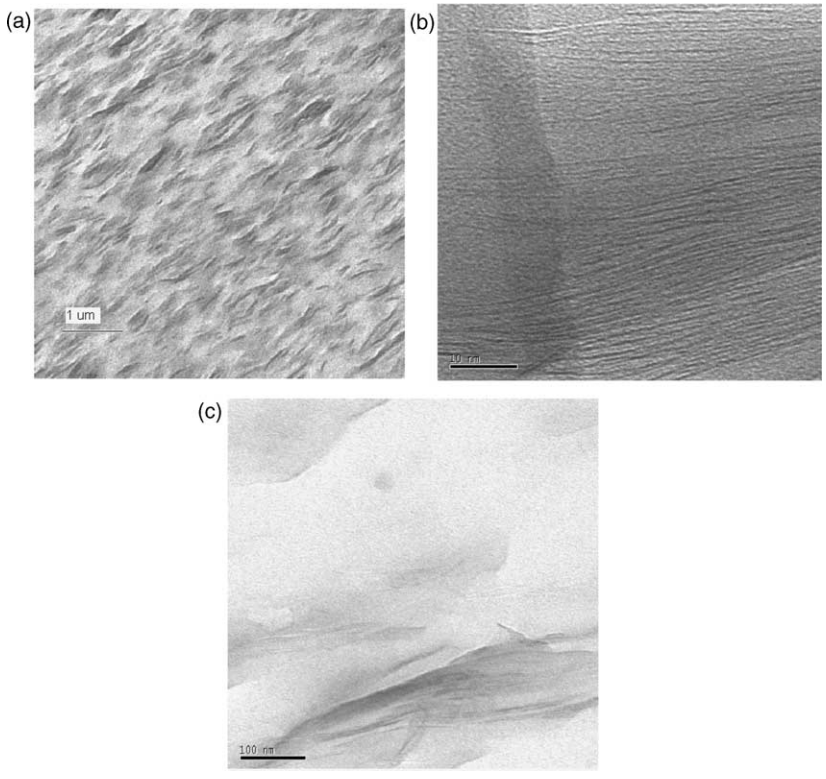

Fig. 3. TEM of the PLA-25A extruded blown film: (a) low magnification, (b) medium magnification, (c) low magnification.

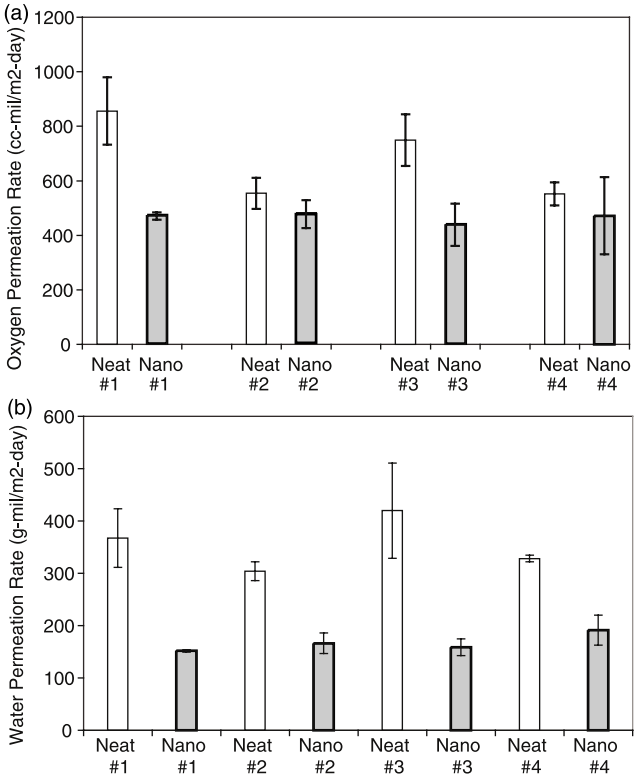

Fig. 4. MOCON permeation data: (a) oxygen and (b) water vapor transmission.

water across the films is decreased. For the MLS particles, the molecular mobility is reduced due to the intercalation of the chains into galleries between the platelets. As was the case for oxygen, the water vapor barrier properties of the nano-PLA films were essentially independent of processing. The impact of screw speed and feed rate on the permeation rate of the neat-PLA films to water vapor was similar to that observed for oxygen permeation rate. However, whereas the general pattern was the same, the magnitude of the changes in water vapor permeation rate was much smaller than that observed for oxygen permeation rate [31].

3.3. Thermal properties

Polymer/MLS nanocomposites can demonstrate enhanced thermal properties over the neat polymer. The degradation process is often shifted to higher temperatures when MLSs are incorporated into the matrix. The explanation for this behavior is not entirely known, but is theorized by Zanetti et al. [40] to result from the increased diffusion pathway of combustion products caused by the MLS layers. A representative TGA curve for the neat- and nano-PLA samples (Sample no. 2: prepared at a screw speed of 110 rpm and a feed rate of 40.5 g/min) is illustrated in Fig. 5. Similar TGA curves were obtained for all the neat- and nano-PLA films. The onset of thermal degradation was approximately 9 °C higher for the nanocomposite than for the neat PLA and was attributed to the addition of the MLS to the polymer matrix. This compares to the shifts that Paul observed for the PLA/MLS 25A (3%)/polyethylene glycol plasticizer nanocomposites [21], however, we have obtained as high as 80 °C shifts in thermal stability for low density polyethylene/MLS nanocomposites [41].

Representative DSC thermograms for the blown films are presented in Fig. 6, (a) first heat (b) second heat data. The values of all samples are tabulated in Table 3. The T_g of both the neat and nano-PLA films was minimally affected by minor changes in the screw speed (i.e. residence time in the extruder). Both the as-processed sample (first heat) and the post-annealed sample (second heat) are analyzed. The as-processed sample is examined in an effort to correlate the barrier properties to morphological changes in the film. As seen in the figure, in the as-processed sample, the degree of non-equilibrium structure was underscored by the large enthalpy relaxation peak that followed the glass transition. The peak was more significant in the neat samples compared to the nanocomposites and the peak area showed higher values in the neat resins compared to the corresponding nanocomposites. Cold crystallization and melting temperatures were not notably significant between the neat resins and the nanocomposites. As can be seen in

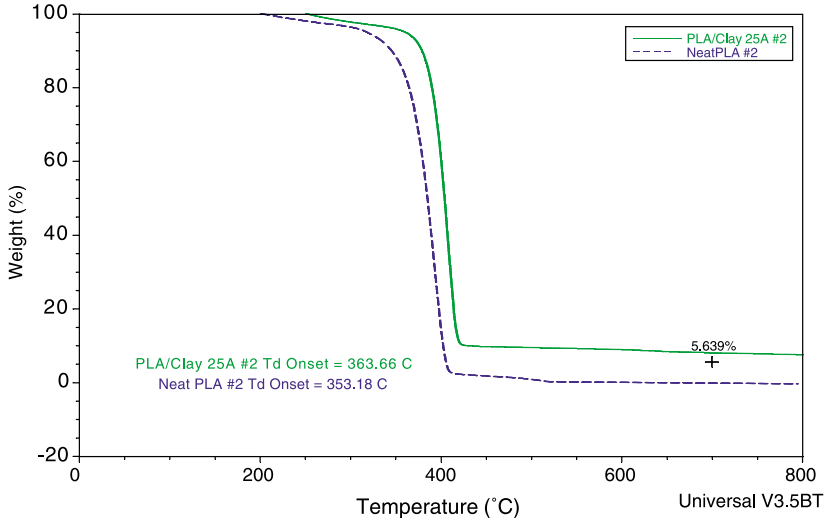

Fig. 5. TGA of neat PLA and nano-PLA/MLS.

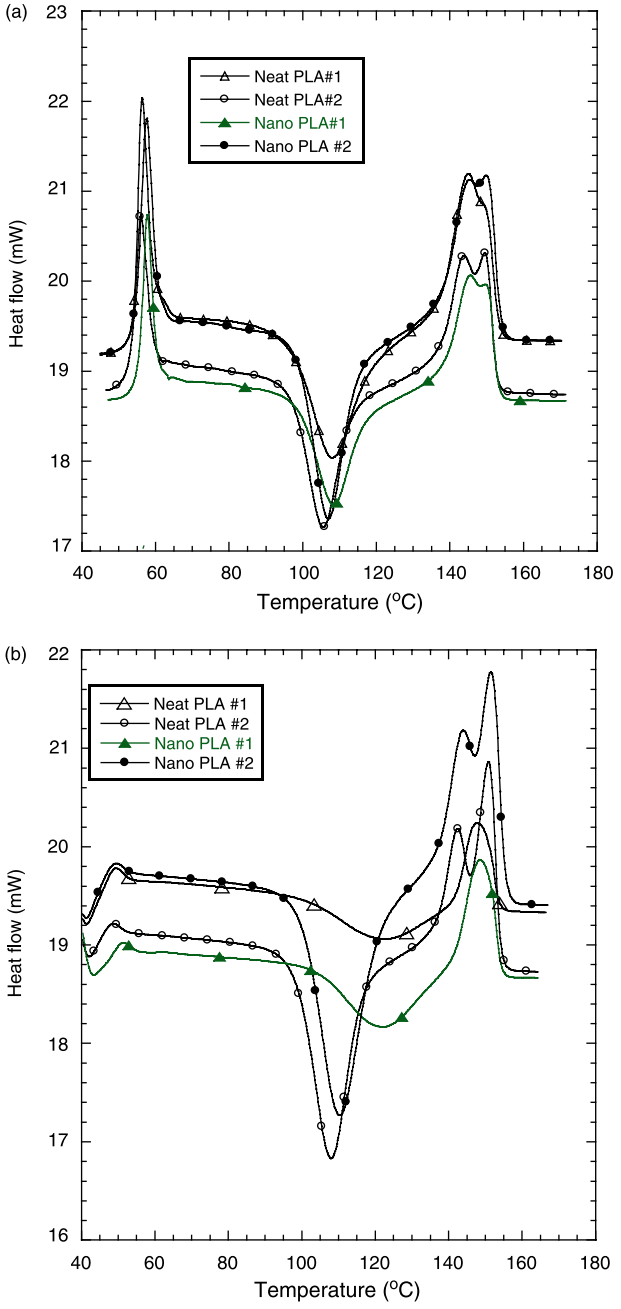

Fig. 6. Representative DSC data for PLA and its nanocomposites at different residence times: (a) first heating scan and (b) second heating scan.

Fig. 6a and b, the PLA shows a soft shoulder which is rendered sharper by the introduction of MLS.

After annealing at 180 °C and slow cooling to 30 °C, the samples were reheated, with the subsequent DSC scan (Fig. 6b) demonstrating that the cold crystallization peak was retained. However, a very substantial difference now occurred in the thermal history response of the nanocomposites. The molecular reordering in the amorphous phase during the first heating scan results in the absence of the enthalpy relaxation peak following the glass transition temperature. Chain reorganization also results in the cold crystallization temperatures shifting to higher temperatures with some increase in peak areas. There was no significant change in the melting peak temperatures or

Table 3
Summary of DSC dat of PLA and PLA nanocomposites

(a) Summary of first and second heat DSC data of PLA and PLA nanocomposites

Sample	Area of enthalpy relaxation peak	First heating scan		Second heating scan	
		Peak, T_m (°C)	ΔH (J/g)	Peak, T_m (°C)	ΔH (J/g)
Neat PLA no. 1	15	145	15	147	10
Nano PLA no. 1	13	144, 149	16	148	12
Neat PLA no. 2	16	144, 150	23	143, 150	28
Nano PLA no. 2	11	145, 150	25	143, 151	34
Neat PLA no. 3	15	144	25	145, 154	31
Nano PLA no. 3	12	150	27	143, 151	32
Neat PLA no. 4	14	146	26	148	28
Nano PLA no. 4	12	150	27	147, 152	33

(b) Summary of first and second heat cold crystallization data obtained from DSC of PLA and PLA nanocomposites

Sample	First heating scan		Second heating scan	
	Peak, T_{cc} (°C)	ΔH_{cc} (J/g)	Peak, T_{cc} (°C)	ΔH_{cc} (J/g)
Neat PLA no. 1	111	15	121	15
Nano PLA no. 1	105	19	121	26
Neat PLA no. 2	105	24	108	33
Nano PLA no. 2	108	30	110	38
Neat PLA no. 3	105	31	107	26
Nano PLA no. 3	106	21	111	31
Neat PLA no. 4	111	25	121	28
Nano PLA no. 4	108	23	115	32

melting enthalpies. Most samples also indicated a sharper peak doublet in the melting peak for both the neat and nanocomposite films.

The supermolecular structure was also analyzed by polarized optical microscopy as shown in Fig. 7a and b. Following the controlled thermal history (annealing at 115° for 1 h followed by slow cooling to room temperature) PLA and the nanocomposite samples were examined. The PLA samples showed crystalline aggregates well distributed in the film seen as bright regions due to optical birefringence. The corresponding nanocomposites, however, show that for the same annealing time, the spherulitic dimensions are considerably larger but individual lamella have a hindered growth appearing as amorphous fan shaped aggregates.

We probe an influence of crystallization on the permeation of the PLA nanocomposite. Clearly, the as-processed nanocomposites have not developed a degree of crystallinity within the process environment. The post-annealed samples, for instance, exhibit a significant increase in enthalpy over the as-processed sample. However, it is clear that the decreased enthalpy relaxation, lower and narrower cold crystallization temperatures indicate a degree of densification in the samples after thermal history than in the as-processed samples. Given the lack of distinction between the neat and nano-samples with the same process history, we can surmise that the improved permeation rates of the PLA nanocomposites is reflective of the MLS dispersion and not due to improved crystallization in the matrix. Recall Fig. 3a showing a well-dispersed intercalated nanocomposite.

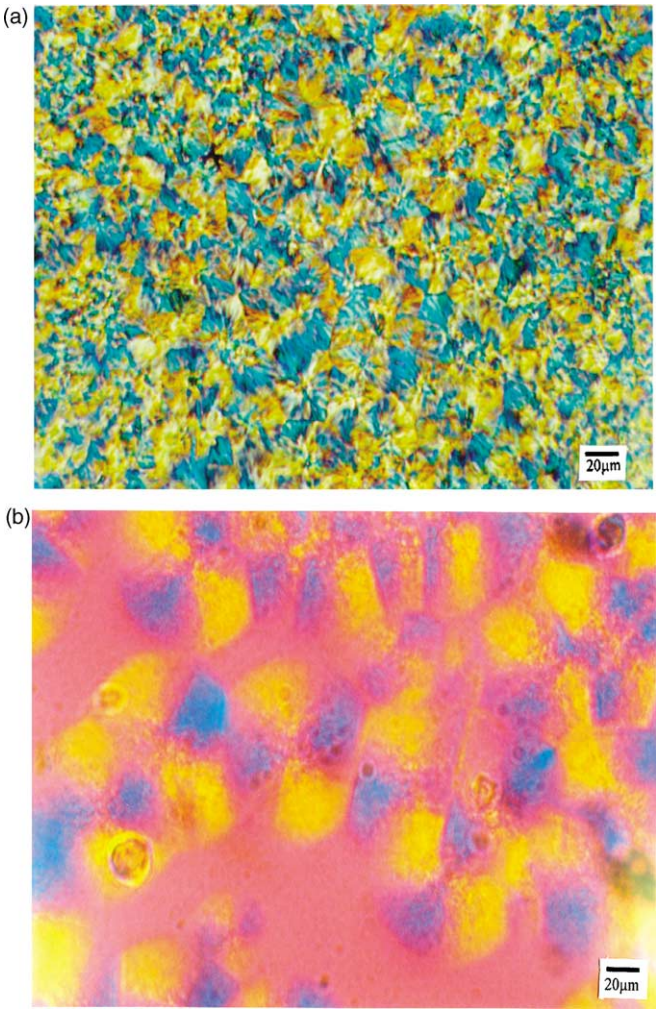

Fig. 7. Optical microscopy of PLA and PLA/MLS: (a) neat no. 1, (b) nano no. 1.

3.4. Mechanical properties

All data here is shown in the machine direction. Generally speaking, the processing conditions did not appear to have a direct influence on the mechanical properties of the films. As observed from the GPC data [31], the PLA in nanocomposite films processed at the highest screw speeds exhibited a 17% loss in molecular weight, a result of increased heat and shearing effects. Nanocomposite films processed at the lowest screw speeds exhibited an average molecular weight loss of only 6%.

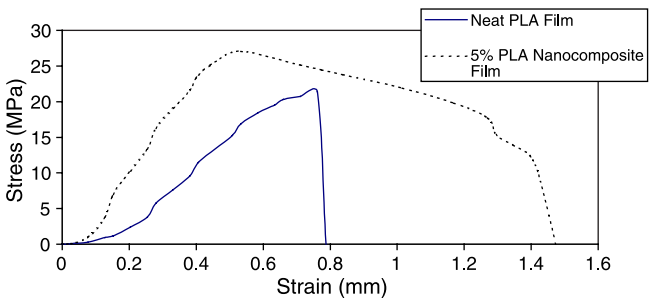

Fig. 8. Typical stress–strain curve for PLA and PLA/MLS.

Organically modified MLSs can act as excellent reinforcing agents for polymer materials if dispersed correctly in the polymer matrix. The dispersed MLS platelets allow for stress transfer to the high-surface area MLS reinforcements, strengthening and toughening the polymer [2]. This type of behavior was exhibited in our PLA/MLS nanocomposite films (Figs. 8 and 9). A typical stress–strain curve for the pure PLA and PLA nanocomposite films is shown in Fig. 8. On average, the Young's modulus for the nano-PLA samples (Fig. 9a) was about 30–40% greater than that of the neat polymer. However, incorporation of the MLS into the PLA matrix produced no significant change in the tensile strength of the resulting films (Fig. 9b). Adding a filler to a plastic usually would decrease the elongation significantly, but this was not the case with the MLS in this system. Indeed, elongation was about 16–40% greater for the nano-PLA films than for the neat films (Fig. 9c). Giannelis has recently reported on dramatic enhancements in elongation to break (140%) and toughness (700%) for a nanocomposite consisting of polyvinylidene fluoride (PVDF)

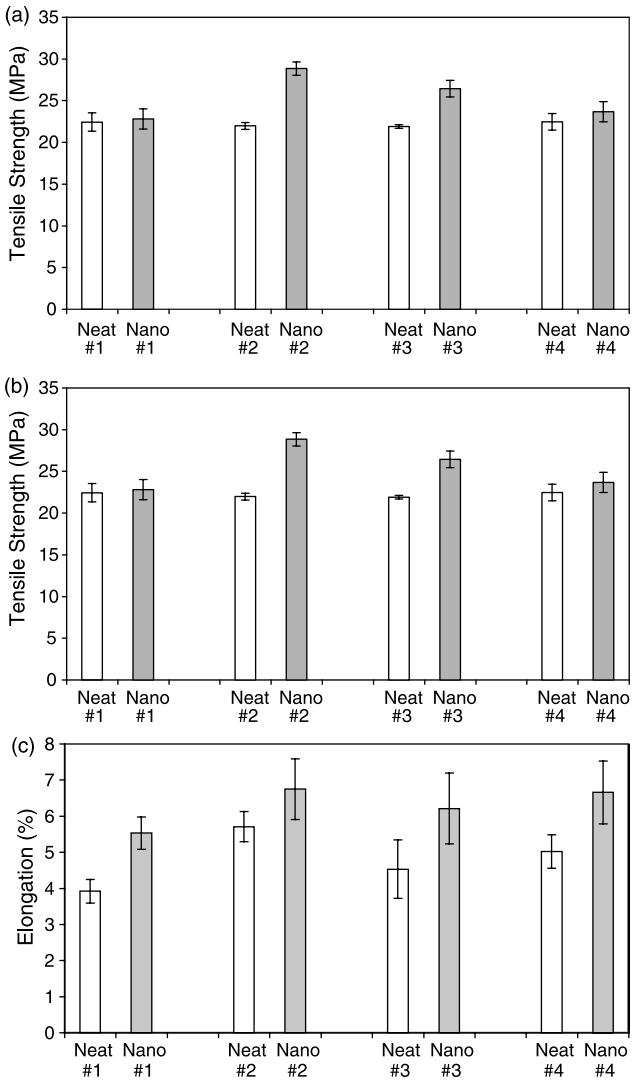

Fig. 9. Mechanical properties of the PLA and PLA nanocomposites (a) Young's modulus of PLA and PLA/MLS, (b) tensile strength of PLA and PLA/MLS, and (c) elongation of PLA and PLA/MLS.

and a surface modified MLS [42]. No improvement in toughness was observed for the non-modified MLS/PVDF system.

Although the PLA/MLS system did not see these highly significant enhancements, the toughness is at least maintained in the PLA/MLS nanocomposites unlike other filled polymeric systems. Giannelis attributes this enhancement to a new energy-dissipation mechanism during deformation and that the MLS induces structural and morphological changes that increases chain mobility as compared to micrometer-size fillers [42]. These results also complement prior work by one of us on polypropylene and polyethylene nanocomposites [43]. In both those systems, the improvement in strain to failure was correlated to the development of a bimodal crystallite distribution. Recall Fig. 6 where a peak doublet was evident in some of the melting transition of the nanocomposites.

3.5. Bio-environmental degradability

Results obtained for the unamended soil and the positive control (i.e. the soil amended with cellulose powder) during a 180-day soil test exposure are presented in Fig. 10. Carbon dioxide production in the control soil is a result of mineralization of the native soil organic matter, which proceeded in a linear fashion at a rate of about 0.13 mg CO_2–C d^{-1} throughout the 180-day test exposure. Mineralization of the positive control (cellulose) proceeded slowly at first (with a lag period of about 8 days) but then increased rapidly from about Day 8 to Day 21. After Day 21, net CO_2 production continued to increase in a near-linear fashion for another 9 weeks—though at a much slower rate—before approaching a plateau at about Day 104. The time required to achieve 60% net mineralization was ca. 76 days, which was well within the 180-day time-frame set out in the ASTM standards.

Net mineralization curves for the various PLA and PLA/MLS nanocomposites are presented in Fig. 11. In general, the net mineralization curves are characterized by a small, but relatively rapid increase in CO_2 production during the first 7–10 days of the test exposure, followed by a much slower, but relatively constant, increase in net CO_2 production during the remainder of the exposure. During this latter phase, net mineralization of both the neat and nanolayered materials was best described using a linear model, with rate constants ranging from about 0.005 to 0.013 mg CO_2–C d^{-1} (Table 4) The initial (more rapid) mineralization phase was most likely a result of microbial attack along exposed end groups as well as the mineralization of low molecular weight fragments in the polymer matrix and the acetyltriethyl citrate plasticizer.

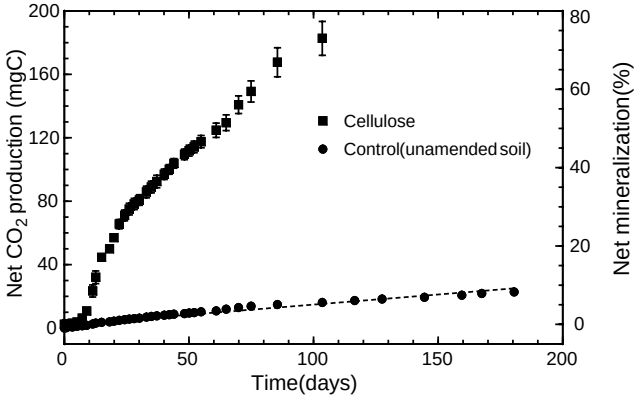

Fig. 10. Carbon dioxide produced by the control (unamended) soil and soil amended with cellulose powder (i.e. the positive control) at 22 °C and 55±5% water-holding capacity.

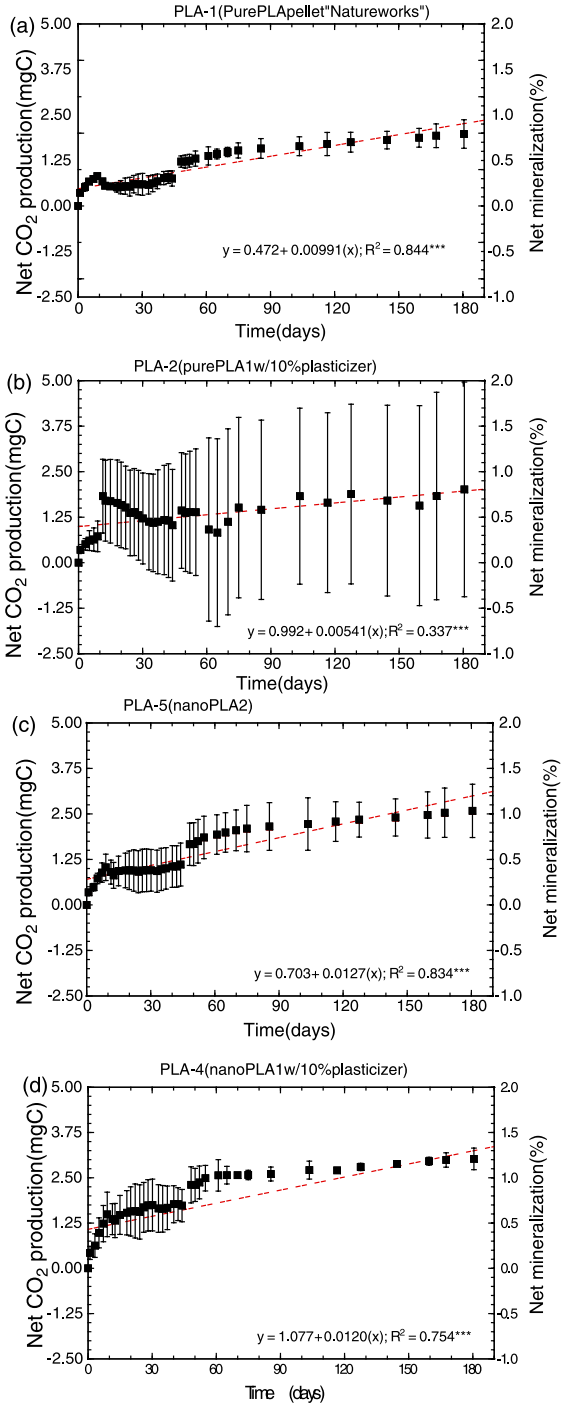

Fig. 11. Net mineralization of (a) PLA, (b) PLA/CE, (c) PLA/MLS, and (d) PLA/MLS/CE powders in soil at 22 °C and 55±5% water-holding capacity.

Table 4
Mineralization of the PLA-clay nanocomposite films and positive control (cellulose) during a 180-day test exposure in soil at 22±1 °C and a moisture content of 55±5% Whc

Test material	Lag[a] (days)	Mineralization			r_{pdp}[b] (mg C d^{-1})	t_{60}[c]
		Max-CO_2C[d] (mg)	ThCO_2 (%)	RBI[e]		
Cellulose powder	8	175.5±10.9	70.5±4.4	–	4.13±1.19 (1.51±0.07)[f]	59
Neat PLA	IND	2.07±0.36	0.83±0.14	0.01	0.010±0.001	IND
PLA/CE	IND	2.51±2.18	1.01±0.87	0.01	0.005±0.003	IND
PLA/MLS	IND	2.63±0.73	1.06±0.29	0.02	0.013±0.002	IND
PLA/MLS/CE	IND	2.93±0.83	1.28±0.18	0.02	0.012±0.002	IND

[a] Time required for net mineralization to reach 10% of the max-CO_2. *Note:* In those cases where the net mineralization curve did not reach a plateau, the Lag was defined as the time required for net CO_2-C evolution to reach 5% ThCO_2. Ind: indeterminate.
[b] Average rate of mineralization during the primary degradation phase: defined as the slope of the linear least-squares regression line plotted between the end of the lag period and start of the plateau region (i.e. the point where net mineralization = two-thirds max-CO_2). *Note:* for the PLA samples there was no distinct lag period and the linear model gave the best fit to the net mineralization curves; therefore, the rate constant was calculated as the slope of the linear least-squares regression equation.
[c] Time required for substrate mineralization to reach 60% ThCO_2. Ind: indeterminate.
[d] The maximum amount of CO_2-C evolved during the 180-day test exposure.
[e] Relative biodegradation index = (% mineralization of the test sample–% mineralization of the positive control); positive control = cellulose.
[f] Values in parentheses are the rate (± the 95% confidence interval) during the slower mineralization phase (i.e. between days 22 and 85).

These results are similar to those obtained by Kouloungis [44] and Mizuno et al. [45], but contrast sharply with the results commonly obtained in more biologically active composting environments [16,35]. This reflects the facts that the environmental degradability of PLA is due primarily to hydrolysis and microbial action, and that compost environments generally much moister and warmer than soils are an especially rich source of microorganisms. Soil environments, on the other hand, are generally characterized by environmental conditions that do not favor the hydrolysis of PLA and PLA-degrading microorganisms are only sparsely distributed in soil environments [46]. As a result, there is only minimal ester cleavage and the formation of oligomer fragments—which are more readily biodegradable—is much lower in soils than in composts. Hence, it is to be expected that the biodegradation of PLA (or PLA/MLS nanocomposites) will be much slower in soil environments.

An analysis of variance revealed that net cumulative mineralization of the PLA/MLS (Fig. 11c) was greater than that of the neat PLA (Fig. 11a). Likewise, the rate of mineralization of the PLA/MLS (while still quite low) was significantly greater than that of the neat PLA. Ray et al. [16] observed a similar (though much larger) increase in the biodegradability of PLA/MLS nanocomposites under composting conditions. They suggested that terminal hydroxylated edge groups on the silicate layers was one of the factors responsible for this behavior. It was assumed (and later confirmed) that the hydroxy groups initiated heterogeneous hydrolysis of the PLA matrix after absorbing water from the compost.

Because the neat-PLA and nano-PLA films all contained the biodegradable plasticizer acetyltriethyl citrate, comparisons could not be made to a pure PLA film because of its the problems during processing in the absence of plasticizer. However, biodegradation testing using powdered samples with and without plasticizer was conducted. Addition of plasticizer to the PLA matrices (i.e. either the neat PLA or PLA/MLS composite) had no significant effect on either cumulative net mineralization (Fig. 11b and d) or the rate of mineralization of the resulting PLA composites (Table 4). Similar results were observed for plasticized PLA films buried in soil [12]. Indeed, significant mineralization of the plasticizers (triethyl citrate and acetyltri-*n*-butyl citrate) was observed only at very high plasticizer contents (e.g. 20% or more).

4. Conclusions

Plasticized poly(L-lactide) Cloisite 25A MLS nanocomposites were prepared using the blown-film processing method. The addition of MLS platelets did not severely affect the stability of the blown-film bubble and processing was similar to that of the plasticized PLA film without MLS. WAXD indicated that variations in screw speed and feeding rate in the process did not affect the dispersion of the MLS platelets in the polymer matrix significantly, nor did it influence the final properties of the blown-film nanocomposites. The diffraction patterns did indicate that intercalation was present in the films and that the MLS was well dispersed throughout the PLA matrix. The nanocomposite films formed showed a high degree of barrier improvement to water vapor and oxygen as well as improved thermal degradation properties and mechanical properties. The thermal properties did not vary significantly for the neat PLA in comparison to the nanocomposites. Crystallization of the PLA did not appear to influence the barrier properties of the nanocomposites. Biodegradation testing in soil showed slow rates of biodegradation for both the pure PLA and the PLA nanocomposites. Crystallization kinetic studies are underway for this system.

Acknowledgements

The Army thanks the Strategic Environmental Research and Development Program (SERDP) for the funds for this project. The authors are also grateful to: Dr Bert Powell and Mr Randy

Chapman from Southern Clay Products for supplying the montmorillonites and the X-ray data; Dr Michael Mang of Cargill Dow for supplying the PLA, Elizabeth Culhane from the U.S. Army Natick Soldier Center for technical support and Siddhi Pendse from University of North Texas for DSC and POM measurements.

References

[1] Giannelis EP. Adv Mater 1996;8:30.
[2] Messersmith PB, Giannelis EP. Chem Mater 1994;6:1719.
[3] Lebaron P, Wang Z, Pinnavaia TJ. Appl Clay Sci 1999;15:12.
[4] Giannelis EP. Appl Organometal Chem 1998;12:675.
[5] Krishnamoorti R, Giannelis EP. Macromolecules 1997;30:4097.
[6] Pinniavaira TJ, Beall GW, editors. Polymer–clay nanocomposites. New York: Wiley; 2001. p. 1–290.
[7] Yoon PJ, Hunter DL, Paul DR. Polymer 2003;44:5323.
[8] Dennis HR, Hunter D, Chang D, Kim S, White JL, Cho JW, et al. Polymer 2001;42:9513.
[9] Lunt J. Polym Degrad Stab 1998;59:146.
[10] Ke T, Sun XS. J Appl Polym Sci 2003;88:2948.
[11] Martin O, Averous L. Polymer 2001;42:6209.
[12] Labrecque L. Master's Degree Thesis in plastics engineering. Lowell, MA: University of Massachusetts Lowell; 1994.
[13] Ogata N, Jimenez G, Kawai H, Ogihara T. J Polym Sci, Part B: Polym Phys 1997;35:389.
[14] Ray SS, Yamada K, Okamoto M, Ueda K. Nano Lett 2002;2:1093.
[15] Ray SS, Maiti P, Okamoto M, Kazunobu Y, Ueda K. Macromolecules 2002;35:3104.
[16] Ray SS, Yamada K, Ogami A, Okamoto M, Ueda K. Macromol Rapid Commun 2003;23:943.
[17] Ray SS, Yamada K, Okamoto M, Ueda K. Polymer 2003;44:857.
[18] Ray SS, Yamada K, Okamoto M, Fujimoto Y, Ogami A, Ueda K. Polymer 2003;44:6633.
[19] Nam JY, Ray SS, Okamato M. Macromolecules 2003;36:7126.
[20] Ray SS, Yamada K, Okamoto M, Ogami A, Ueda K. Chem Mater 2003; 15:1456.
[21] Paul MA, Alexandre M, Degee P, Henrist C, Rulmont A, Dubois P. Polymer 2003;44:443.
[22] Pluta M, Galeski A, Alexandre M, Paul MA, Dubois P. J Appl Polym Sci 2002;86:1497–506.
[23] Vasanthan N. Notes of research. New York: TRI/Princeton Press 1999; #527: 2000.
[24] Chang JH, Yeong U, Cho D, Giannelis EP. Polymer 2003;44:3715.
[25] Maiti P, Yamada K, Okamoto M, Ueda K, Okamoto K. Chem Mater 2002; 14:4654.
[26] Cook RL, Elliott B, Luebben S, Myers A, Smith B. Polym Mater Sci Eng 2001;85:159.
[27] Krikorian V, Pochan DJ. Macromolecules 2004;37:6480.
[28] Lucciarini JM, Ratto J, Koene BE, Powell C. Annu Technic Conf Soc Plast Eng 2002;60(2):1518.
[29] Deanin R. Polymer structure, properties and applications. Boston, MA: Cahners Books; 1972 p. 239.
[30] Massy LK. Permeability properties of plastics and elastomers. second ed. A guide to packaging and barrier materials. New York: Plastics Design Library; 2003 p. 49.
[31] Thellen CT. Master's Degree Thesis in plastic engineering. Lowell, MA: University of Massachusetts Lowell; 2003.
[32] Thellen CT, Orroth C, Ratto J. Seventh annual green chemistry and engineering conference [CD-ROM]. The National Academies, Washington, DC; 2003. Paper No. 2.
[33] Bartha R, Pramer D. Soil Sci 1965;100:69.
[34] American Society for Testing and Materials. Annual Book of ASTM Standards. vol. 08-03. West Conshoshocken, PA: ASTM; 2001. Standard D 5988.
[35] Farrell RE, Adamczyk TJ, Broe DC, Lee JS, Briggs BL, Gross RA, et al. In: Gross RA, Scholz C, editors. Biopolymers from polysaccharides and agroproteins. ACS Symposium Series 786. Washington, DC: American Chemical Society; 2001. p. 337.
[36] Bissot TC. In: Koros WJ, editor. ACS Symposium Series Barrier Polymers and Structures. Washington, DC: American Chemical Society; 1989. p. 225.
[37] Bharadwaj RK. Macromolecules 2001;34:9189.
[38] Nielson LEJ. Macromol Sci Chem 1967;A1:929.
[39] Gerlowski L. In: Koros WJ, editor. ACS Symposium Series Barrier Polymers and Structures. Washington, DC: American Chemical Society; 1989. p. 180.
[40] Zanetti M, Camino G, Mulhaupt R. Polym Degrad Stab 2001;74(3):413.
[41] Ratto J, Culhane E, Froio D, Thellen C, Orroth C, Lucciarini J. Annual technical conference SPE; May 2005.
[42] Shah D, Maiti P, Gunn E, Schmidt DF, Jiang DD, Batt CA et al. Advanced Materials; 16(14):1173–1177.
[43] Ranade A, Nayak K, Fairbrother D, D'Souza NA. Polymer 2005;46(18): 7323.
[44] Kouloungis NR. MSc Thesis, University of Massachusetts Lowell, Lowell, MA; June 1996.
[45] Mizuno W, Sano M, Song CJ, Nakatani T, Yoshida T, Takeuchi S. Kobunshi Ronbunshu 2003;60:622.
[46] Pranamuda H, Tokiwa Y, Tanaka H. Appl Environ Microbiol 1997;63(4): 1637–40.